RSC Advances

ROYAL SOCIETY OF CHEMISTRY

www.rsc.org/advances

RSC Advances

RSCPublishing

ARTICLE

Self-Assembly of DNA Wrapped Carbon Nanotubes and Asymmetrical Cyanine Dyes into Fluorescent Nanohybrids

O. Cavuslar[a] and H. Unal[a]

ite this: DOI: 10.1039/x0xx00000x

Received ooth January 2012,
Accepted ooth January 2012

DOI: 10.1039/x0xx00000x

www.rsc.org/

Light absorbing and emitting nanohybrid materials constructed from single stranded DNA, asymmetrical cyanine dyes and carbon nanotubes are presented. Asymmetrical cyanine dyes interact strongly with carbon nanotubes through noncovalent binding resulting in light absorbing nanoarrays for which the fluorescence emission is quenched. On the other hand, when carbon nanotubes are wrapped with single stranded DNA, a unique scaffold is formed on which asymmetrical cyanine dyes can self-assemble with increased quantum yields resulting in fluorescent nanohybrids. These three-component nanohybrid materials can absorb and emit light at desired ranges of the spectrum and are the first example where fluorescent dyes light up when bound to carbon nanotubes as opposed to being quenched. The DNA/carbon nanotube/dye nanohybrids are shown to be energetically favored, consistently formed self-assembled nanostructures that are obtained independent of the order of addition of components. These nanohybrid materials have been characterized for their binding stoichiometry and thermal stability by utilizing absorbance and fluorescence spectroscopy; furthermore, their fluorescence has been visualized with confocal microscopy. While the method presented here is valuable for fluorescent labeling of carbon nanotubes for biomedical applications, these nanohybrid materials are also potential candidates for photoactive bionanodevices as light harvesting systems and optical sensors.

1 Introduction

Carbon nanotubes (CNTs) as one of the most appealing and extensively researched materials of nanotechnology are often subject to functionalization in order to fully utilize their intrinsic properties and expand their potential applications in various fields. While functionalization of CNTs is critical for the debundling of CNTs into individual nanotubes to improve their processability, it is also desired for imparting new functions to CNTs and creating novel hybrid materials. CNTs can be functionalized with various molecules through covalent or noncovalent binding resulting in CNT hybrids that synergistically carry properties of both components. [1-3] Noncovalent functionalization of sidewalls of CNTs through π-π stacking and hydrophobic interactions is especially attractive as the electronic structure of CNTs is not disturbed and the key properties are preserved. Small molecules[4-6], biomolecules[7-9], and polymers[10-13] have been attached to CNTs through noncovalent binding interactions resulting in CNT conjugates that can be utilized in applications ranging from field effect transistors to biosensors; from drug delivery to chemical sensors.[3]

One of these approaches that attracts considerable attention is the functionalization of CNTs with fluorescent molecules. Efforts to fluorescently label CNTs mainly originate from the need to detect and visualize CNTs in biologically relevant environments for biomedical applications. Routinely used characterization methods such as electron microscopy and Raman spectroscopy are not suitable when interactions of CNTs with cells or other biological molecules need to be studied. On the other hand, optical microscopy that is the correct choice for biological applications suffers from low resolution at the size range of CNTs and can be utilized for visualization only if CNTs are fluorescently tagged. Therefore, novel methods to prepare fluorescently labeled CNTs are highly desired in order to improve the efficacy of CNTs in biomedical applications. In addition, CNTs functionalized with fluorescent molecules are also attractive for their potential as electron donor/acceptor systems for artificial photosynthetic devices[14, 15] or as optical sensors.[16, 17] The unique electronic structure of CNTs combined with the tunability of organic fluorophores can result in novel photoactive hybrid materials.

Interactions of CNTs with several fluorescent molecules including fluorescein[18, 19], symmetrical carbocyanines[20], anthracene[21] pyrene[22], porphyrin[23, 24], quantum dots[25], fluorescent polymers[26-28] and other chromophores[29] have been studied. The main obstacle in directly labeling CNTs with fluorophores is the quenching of fluorophores upon binding to CNTs. Noncovalent interactions that allow the adsorption of fluorophores on CNTs such as π-stacking, Van der Waals, and hydrophobic interactions lead to electron and energy transfer causing decrease in fluorescence emission.[30, 31] A new fluorescent labeling platform is desired in which fluorophores do not lose their fluorescence signal when they interact with CNTs but instead become highly fluorescent and allow the formation of fluorescently labeled CNTs.

In order to develop a simple and effective method to fluorescently label CNTs we focused on interactions of asymmetrical cyanine dyes with CNTs. Asymmetrical cyanine dyes, mainly used as fluorescent probes for DNA, are unique in the sense that they switch from a quenched, dark state to a fluorescent state when they are constrained in a restrictive environment such as a viscous solution or between the base pairs of double stranded DNA.[32, 33] Due to this light-up behaviour, asymmetrical cyanine dyes have strong signal to noise

ratio and are attractive for the labeling of nucleic acids, peptides, and proteins.[34-36] Herein, we investigated whether asymmetrical cyanine dyes can exhibit a similar light-up behaviour when they interact with CNTs and alternatively with DNA wrapped CNTs. A novel method to prepare strongly absorbing, highly fluorescent asymmetrical cyanine dyes/CNT nanohybrids that can be utilized in fluorescence detection of CNTs and also as novel materials for photonic devices is presented.

2 Experimental

2.1 Materials

Asymmetrical cyanine dyes YO-PRO-1 (Y3603), TO-PRO-1 (T3602), YOYO-1 (Y3601), and TO-PRO-3 (T3605) were purchased from Life Technologies. TO was purchased from Sigma Aldrich. CNTs were purchased from Cheap Tubes Inc. in the form of dry powder. The purity of CNTs as declared by the supplier is >99% for SWNTs, >99% for MWNTs and >60% for DWNTs. ssDNA composed of 20 Guanines, ($Poly(G)_{20}$) was synthesized by Sentromer DNA Technologies, Istanbul, Turkey. Centrifugal filter devices with a 30 kDa cut-off membrane (Microcon-30kDa) were purchased from Millipore.

2.2 Preparation of CNT/asymmetrical cyanine dye nanohybrids

0.5 mL of a dispersal solution containing 0.1 mg/mL CNTs and 30μM asymmetrical cyanine dyes was prepared. The dispersal solution was sonicated with a microprobe (QSonica, Q700) for 30 min with 2 seconds pulse on and 5 seconds pulse off time in ice. The dispersion was ultracentrifuged at 14,000 rpm for 10 min and the supernatant that is the black colored dispersion was transferred into a clean eppendorf tube labeled as CNT/dye dispersion. In order to remove the unbound dye molecules, the dispersion was transferred into a Microcon centrifugal filter device and centrifuged at 14,000 rpm until the filtrate volume is reduced to approximately 50 μL. The filtrate that remains in the filter device was recovered and diluted to 500 μL with water.

2.3 Preparation of ssDNA/SWNT scaffold

A 500 μL of a dispersal solution containing 0.1 mg/mL SWNT and 10 μM $poly(G)_{20}$ in 0.1 M NaCl was prepared. The dispersal solution was sonicated with a microprobe for 45 min with 2 seconds pulse-on and 5 seconds pulse-off time in ice. The dispersion was ultracentrifuged at 14,000 rpm for 10 min and the black supernatant was transferred into a clean eppendorf tube. To remove the free ssDNA that was not bound to SWNT, 30 mM $MgCl_2$ was added to the dispersion to precipitate ssDNA/SWNT conjugates followed by a centrifugation at 2,000 rpm for 2 minutes. The supernatant solution was removed. The black pellet composed of ssDNA/SWNT conjugates was redispersed in 0.5 X TBE buffer (44.5 mM Tris, 1mM EDTA, 44.5 mM Boric acid, pH 8.0) containing 30 mM NaCl and 10mM extra EDTA to complex with residual Mg^{2+}. (10 mM ssDNA was treated exactly the same with $MgCl_2$, to prove that this $MgCl_2$ precipitation does not lead to the precipitation of free ssDNA). Resulting ssDNA/SWNT was tested for the presence of any free ssDNA by using agarose gel electrophoresis. 10 μL of the ssDNA/SWNT conjugate treated with $MgCl_2$ was loaded into a 2% agarose gel along with the same amount of free ssDNA. The samples were run at 135 V for 30 min in 1X TBE buffer. The gel was stained with 0.5 μg/mL ethidium bromide in 1X TBE for visualization and imaged with Biorad Gel Doc EZ System under UV illumination. As an alternative to the $MgCl_2$ precipitation centrifugal filter devices were used to remove unbound ssDNA as explained above.

2.4 Preparation of ssDNA/SWNT/dye nanohybrids with one step sonication:

A dispersal solution containing 0.1 mg/mL dry SWNT powder, 30 μM dye and 10 μM poly $(G)_{20}$ was prepared in water. The solution was ultrasonicated with a microprobe for 30 minutes with a 2 seconds pulse-on and 5 seconds pulse-off time in ice. The resulting dispersion was centrifuged at 14,000 rpm for 10 minutes and the supernatant was transferred into a clean eppendorf tube. The ssDNA/SWNT/dye nanohybrid was filtered by using a Microcon centrifugal filter device with a 30,000 Da cut-off membrane to remove unbound ssDNA, unbound dye and ssDNA/dye conjugates.

2.5 Spectroscopy

Absorbance measurements were made on a Cary 5000 Spectrophotometer. Samples were transferred into quartz cuvettes and scanned 200-800 nm. For SWNT/dye conjugates and SWNT/ssDNA/dye conjugates the spectra was corrected for SWNT absorbance in the measured range by subtracting the absorbance spectrum obtained from SWNT dispersed in Triton X-100. Fluorescence spectra were obtained on a Cary Eclipse Fluorescence Spectrophotometer. Measurements were made in quartz microcuvettes. Dyes and Dye/SWNT conjugates were excited at the following wavelengths: TO: 490 nm, TOPRO-1:490 nm, TO-PRO-3: 620nm, YO-PRO-1: 480 nm, YOYO-1: 480 nm. The bandwidth for excitation and emission was 5nm. For Raman Spectroscopy samples were dried on silicon wafers and measurements were made on a Renishaw in Via Reflex Raman Spectrometer equipped with a 532 nm laser.

2.6 Titration of ssDNA/SWNT scaffold into dye solutions

Aliquots of ssDNA/SWNT dispersion with an ssDNA concentration of 10 μM were titrated into an asymmetrical cyanine dye solution of 1 μM. After each addition the solution in the cuvette is mixed thoroughly and fluorescence intensity is measured. Titration curves were obtained by plotting the fluorescence intensity at the wavelength of maximum emission ($\lambda_{max,e}$) versus the ratio of dye concentration to ssDNA base concentration. ssDNA base concentration was calculated as the ssDNA concentration multiplied with 20 (the number of ssDNA bases on each ssDNA nucleotide). The $\lambda_{max,e}$ for the asymmetrical cyanine dyes were as followed. $\lambda_{max,e}$ TO: 555nm, $\lambda_{max,e}$ TO-PRO-1: 550 nm, $\lambda_{max,e}$ YO-PRO-1: 515 nm, $\lambda_{max,e}$ YOYO-1: 515 nm . Each titration was performed at least three times.

2.7 Titration of dye into ssDNA/SWNT scaffold

Aliquots of asymmetrical cyanine dye solutions having a concentration of 100 μM were titrated into a solution ssDNA/SWNT scaffold of 0.25 μM ssDNA concentration (0.25*20=5μM ssDNA base concentration). The titration curve was obtained by plotting the fluorescence at $\lambda_{max,e}$ versus the ratio of dye concentration to ssDNA base concentration. Each titration was performed at least three times.

2.8 Thermal stability measurements

The thermal stability measurements were taken on the Cary Eclipse spectrophotometer equipped with a Peltier-thermostatted cell holder. The samples were heated from 30^0C to 90^0C with a rate of 1^0C/min, incubated 5 minutes at 90^0C and cooled back to 30^0C with the same rate as the fluorescence at $\lambda_{max,e}$ is monitored.

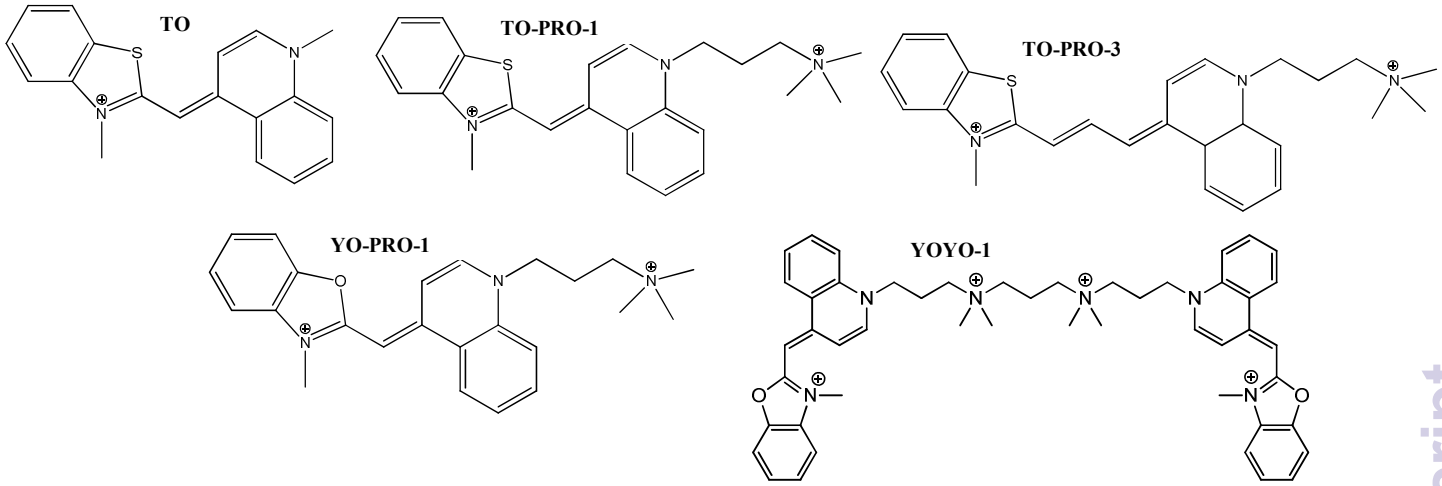

Figure 1 Structures of asymmetrical cyanine dyes studied in terms of their interactions with CNTs

2.9 Confocal Laser Scanning Microscopy

Microscopy samples were prepared on glass slides by dropping 10 µL of the nanohybrid to be visualized on a glass slide. Confocal Laser Scanning Microscopy images were acquired with a Carl-Zeiss LSM 710 confocal microscope equipped with a Plan-Apochromat 63x/1.40 Oil objective. CNTs were excited with a 488 nm laser and images were collected using a 493nm-639 nm filter. DSC images were obtained with excitation of 405 nm laser.

3 Results and Discussion

3.1 Interactions of asymmetrical cyanine dyes with CNTs

Asymmetrical cyanine dyes that were chosen to study in terms of their interactions with CNTs are thiazole orange (TO), its cationic derivatives with a monomethine and a trimethine bridge (TO-PRO-1, TO-PRO-3), cationic derivative of oxazole yellow (YO-PRO-1) and its dimer (YOYO-1). Different charges, sizes and spectral properties of these dyes allow us a systematic investigation of their interactions with CNTs (Figure 1). As an initial step of examining the presence of noncovalent interactions between asymmetrical cyanine dyes and CNTs, solid multi walled CNTs (MWNT) were ultrasonicated with aqueous solutions of dyes. Resulting sonicated mixtures were ultracentrifuged to remove any residues that are not dispersed and to judge on the stability of the resulting dispersions. While MWNTs were not dispersed in water under the same conditions, they were finely dispersed in the presence of dyes as can be seen by the darker colors of the resulting stable mixtures shown in Figure . The ability of dyes to debundle MWNTs and create stable dispersions clearly indicates the presence of strong noncovalent interactions between dyes and MWNTs. The sp^2 hybridized MWNTs and the planar aromatic dyes interact possibly due to π- π stacking interactions resulting in MWNTs decorated with dye molecules. These dispersions were stable over two months without any MWNT precipitation at room temperature, which further indicates the strong nature of the noncovalent interactions.

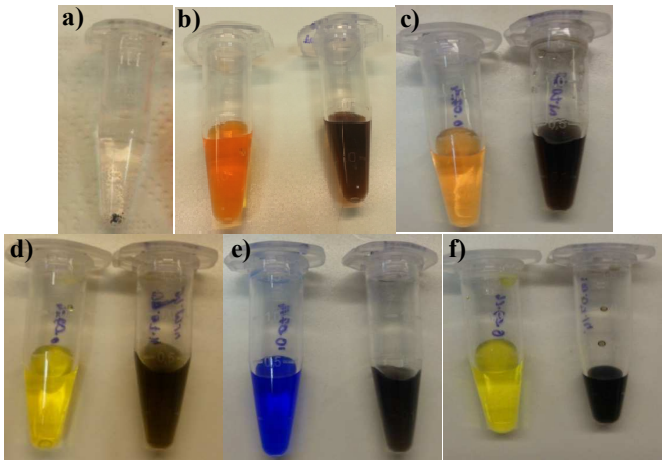

Figure 2 Pictures of MWNT-dye dispersions. a) MWNTs ultrasonicated in water, b-f) MWNTs ultrasonicated in an aqueous solution of dye followed by ultracentrifugation, the supernatant obtained is on the right, and the aqueous dye solution is on the left for comparison. b) TO, c) TO-PRO-1, d) YO-PRO-1, e) TO-PRO-3, f) YOYO-1

Further characterization of binding interactions between dyes and CNTs were conducted with absorbance spectroscopy. Dye/CNT dispersions were treated with centrifugal membrane filter devices to remove unbound dye molecules and to be able to analyze CNT/dye hybrid structures. Figure 3A shows the absorption spectrum of MWNT/YOYO-1 hybrid in comparison to the spectrum of unbound YOYO-1 in water. The absorbance spectrum of the unbound dye has a peak at 460 nm indicative of H-dimers, and another peak at 490 nm indicative of dyes in the monomeric form.[37] As seen on the graph, when the dye is free in solution the dimeric form dominates indicating that the majority of molecules are present as dimers. When YOYO-1 molecules form the hybrid structure with MWNTs, the ratio of monomeric dyes to dimeric dyes changes and the monomeric form dominates. In fact, when YOYO-1 molecules are arranged on the MWNT surface, they are found to be mostly in the monomeric form. Apparently the MWNT structure acts as a scaffold that allows dye molecules to arrange one by one resulting in light

absorbing nanoarrays.

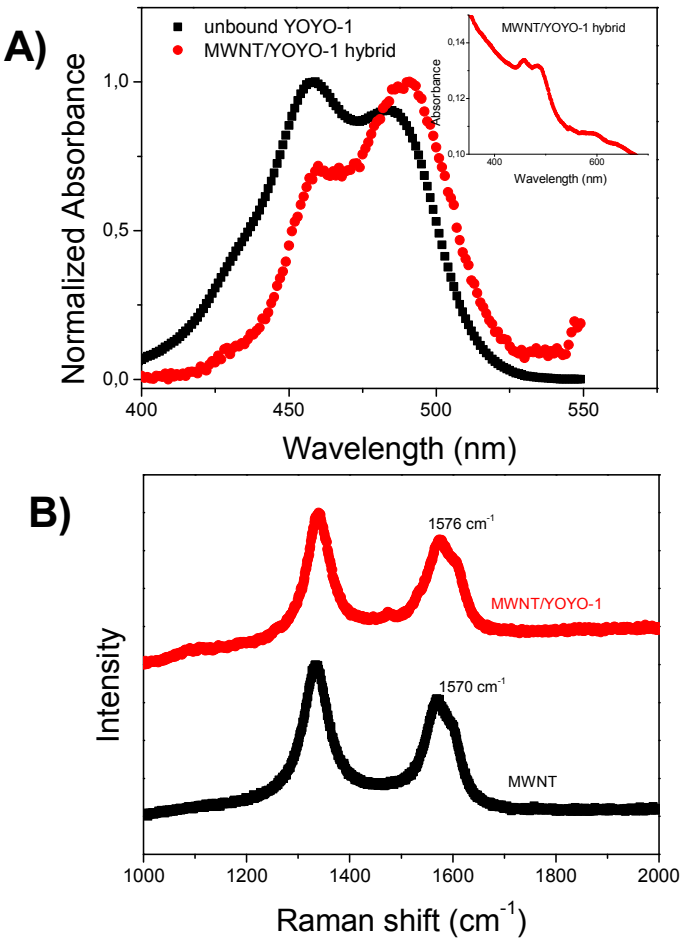

Figure 3 A) Absorption Spectra of free YOYO-1 (black) and MWNT/YOYO-1 hybrid. Spectrum of the hybrid structure is corrected for MWNT absorbance in this wavelength range and both spectra are normalized to stress on the shift of absorption maxima. The Inset shows the original absorbance spectrum of MWNT/YOYO-1 hybrid before MWNT spectrum correction and normalization. B) Raman Spectra of MWNT (black) and MWNT/YOYO-1 hybrid (red) magnified in the G band region.

Similar results indicating that molecules switch from aggregated forms to non-aggregated forms upon binding to MWNTs have been also obtained with other dyes studied in this report. Different sizes and charges depending on the chemical structure of each dye molecule did not have a significant effect on noncovalent binding interactions. TO, TO-PRO-1, TO-PRO-3, and YO-PRO-1molecules were able to noncovalently interact with MWNTs and lead to an arrangement of dyes in which the monomeric forms dominate (SI Figure 1). When the structure, thus the diameter of CNTs were varied by using single walled CNTs (SWNTs), and double walled CNTs (DWNTs) as the scaffold for the binding of asymmetrical cyanine dyes, similar individual light absorbing nanoarrays were obtained (SI Figure 2). These results clearly demonstrated that CNTs can be ideal scaffolds for asymmetrical cyanine dyes to obtain individual CNT/dye nanoarrays with enhanced absorbance in the desired range of the spectrum at which pristine CNTs do not normally absorb light.

The strong binding interaction between asymmetrical cyanine dyes and CNTs was further evidenced with electronic changes on the CNT by using Raman Spectroscopy. Figure B shows Raman spectra of MWNTs in the absence and presence of the bound YOYO-1. Raman shift of the tangential stretch G band of the MWNT alone at 1570 cm^{-1} exhibits an upshift to 1576 cm^{-1} when the dye is bound to MWNT. This shift indicates a change in the electronic structure of sidewalls of MWNT through strong π-π interactions when the MWNT/YOYO-1 hybrid structure is formed. Similar shifts in the G band have previously been reported for noncovalent binding of molecules to CNT surface in the literature.[38, 39] Raman spectroscopy on the CNT scaffold along with the absorbance spectroscopy on asymmetrical cyanine dye molecules demonstrate the formation of strongly interacting nanohybrids that can have tunable light absorption over the visible spectrum.

3.2 Interactions of asymmetric cyanine dyes with ssDNA wrapped CNT:

While nanoarrays resulting from the decoration of MWNTs with asymmetrical cyanine dyes were strongly light absorbing, they did not emit light. The background fluorescence of asymmetrical cyanine dyes did not increase upon binding to CNTs, instead it was further quenched (SI Figure 3). Apparently the close distance between dye molecules and sidewalls of CNTs caused by strong noncovalent interactions lead to electron transfer and thus quenching of dye molecules. Asymmetrical cyanine dyes on the other hand exhibit dramatically enhanced fluorescence when arranged into an optimal binding site that can act as a conformationally restrictive environment yet at the same time prevents quenching by keeping the molecules at a certain distance. Intercalation of asymmetrical cyanine dyes into double stranded DNA by the stacking of aromatic dye molecules between aromatic DNA base pairs exemplifies this phenomenon where the intercalated asymmetrical cyanine dyes are several fold more fluorescent compared to the free dye. Motivated by the strong interactions between asymmetrical cyanine dyes and CNTs and inspired by the DNA intercalation of these dyes, we hypothesized that CNTs wrapped with ssDNA can act as an optimal scaffold for the binding of asymmetrical cyanine dyes and lead to light emitting nanoarrays (Scheme 1).

RSC Advances

RSCPublishing

ARTICLE

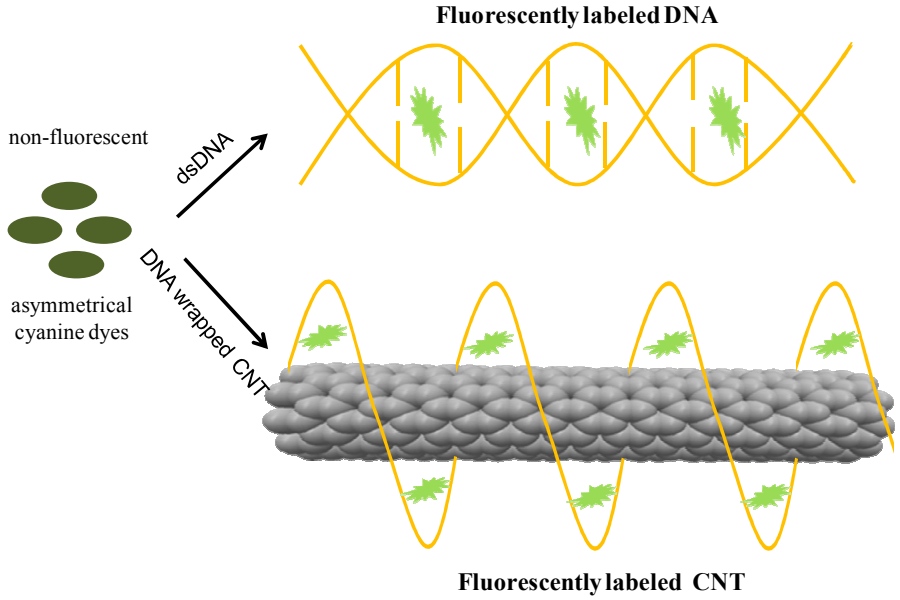

Scheme 1 Labeling of ssDNA wrapped CNTs with asymmetrical cyanine dyes.

The first step to prepare ssDNA/CNT/dye nanohybrids was the preparation of ssDNA wrapped CNT structures. It is well known that ssDNA can bind to CNTs through π-π stacking interactions leading to helical wrapping of CNTs.[40] SWNTs were ultrasonicated in an aqueous solution of ssDNA composed of 20 guanine bases (poly (G)$_{20}$) leading to well dispersed CNTs. The free ssDNA that was not bound to SWNTs were removed by Mg^{2+} ion precipitation[41] and/or ultrafiltration by using a centrifugal filter device of appropriate cut-off size membrane. Agarose gel electrophoresis confirmed that resulting hybrid structures were composed of ssDNA bound to SWNT without any unbound ssDNA (SI Figure 4).

We investigated whether ssDNA/SWNT hybrids can act as a scaffold allowing asymmetrical cyanine dyes to light up as hypothesized. Aliquots of the ssDNA/SWNT scaffold were titrated into an aqueous solution of YO-PRO-1 while the fluorescence was monitored. As ssDNA/SWNT scaffold was added into the dye solution the fluorescence intensity increased up to a point at which all the dye molecules in the cuvette were bound to the scaffold. Figure 4 shows the fluorescence spectrum of the unbound YOPRO-1 dye as compared to the spectrum of the same dye saturated with ssDNA/SWNT scaffold. While the YO-PRO-1 free in solution exhibited only background fluorescence, its fluorescence intensity increased dramatically resulting in fluorescent ssDNA/SWNT/YO-PRO-1 hybrid structures. As we hypothesized, YO-PRO-1 molecules were strongly interacting with the ssDNA/SWNT scaffold via noncovalent interactions and were conformationally restricted within the binding sites resulting in increased quantum yield. Thus, we report for the first time dye molecules that exhibit enhanced fluorescence when bound to SWNT, leading to fluorescently labeled SWNTs.

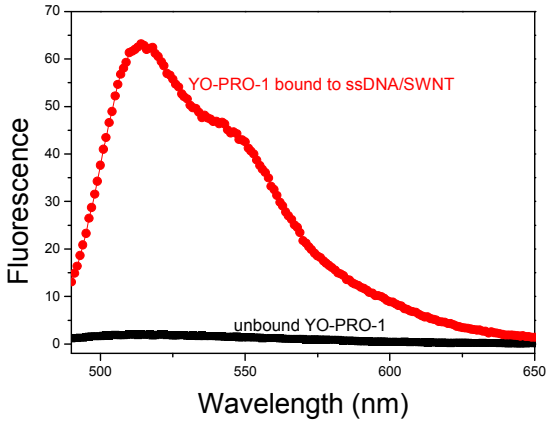

Figure 4 Fluorescence spectra of free YO-PRO-1 (black), and YO-PRO-1 bound to ssDNA/SWNT hybrid (red).

Figure 5 shows the absorbance spectra of resulting fluorescent nanohybrid structures. The ssDNA/SWNT scaffold bound to YO-PRO-1 is strongly absorbing light in the range of the spectrum where the empty ssDNA/SWNT scaffold was not absorbing (Figure 5A). In order to elucidate changes in the electronic structure of YO-PRO-1, absorbance spectrum of the unbound YO-PRO-1 is compared to the spectrum of YO-PRO-1 bound to ssDNA/SWNT and also to the spectrum of YO-PRO-1 bound to ssDNA (Figure 5B). The amount of dye molecules that are in the dimeric form, as indicated by the peak at 460 nm, increased when dye molecules are bound to

ssDNA/SWNT scaffold relative to the amount of dimers in the unbound dye solution. Different shapes of spectra for YO-PRO-1 and ssDNA/SWNT/YO-PRO-1 indicate the presence of noncovalent interactions of individual dye molecules with the ssDNA/SWNT scaffold and clearly evidence the formation of a hybrid structure. When the same amount of dye is bound to ssDNA of the same concentration forming the ssDNA/YO-PRO-1 hybrid, a different ratio of peaks at 460 nm and 481 nm than the three component hybrid was obtained. This difference demonstrates that the ssDNA/CNT scaffold provides a unique environment for the dye molecule in which the dye is not only bound to ssDNA but instead, a hybrid structure composed of CNT, ssDNA and dye is present. Such a three-component self-assembly can be explained with a binding mode that is similar to intercalation where asymmetric cyanine dyes stack between sidewalls of SWNTs and the bases of ssDNA.

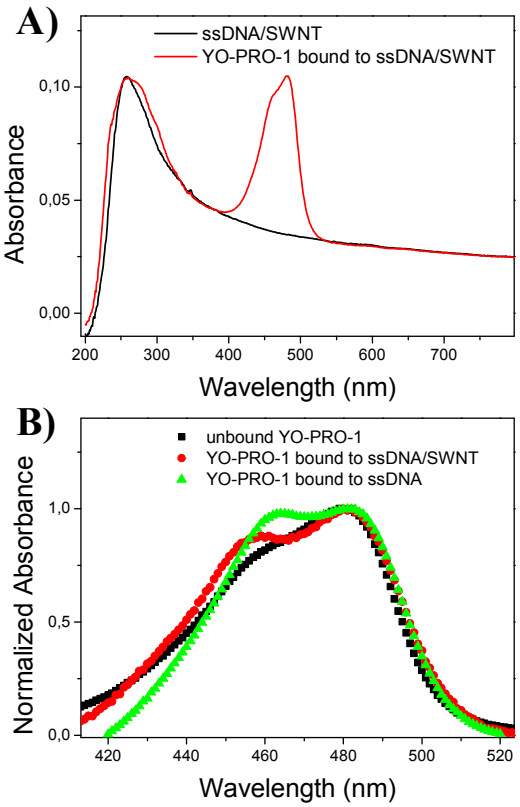

Figure 5 A) Absorbance spectra of ssDNA/SWNT scaffold (black), and YO-PRO-1 bound to ssDNA/SWNT scaffold (red). B) Absorbance spectra of unbound YO-PRO-1 (black), YO-PRO-1 bound to ssDNA/SWNT (red), and YO-PRO-1 bound to ssDNA (red). The concentrations of YO-PRO-1 and ssDNA are the same in all three spectra. Spectra are corrected for ssDNA/SWNT absorbance in the same range and normalized by dividing all data points by the maximum absorbance.

3.3 Binding stoichiometry of asymmetrical cyanine dyes into ssDNA/SWNT scaffold:

In order to speculate on the binding mode with which the YO-PRO-1 molecules arrange on the ssDNA/SWNT scaffold, aliquots of YO-PRO-1 solution were titrated into an ssDNA/SWNT dispersion of known ssDNA concentration. The fluorescence intensity was plotted against the ratio of the dye to ssDNA bases on the scaffold (Figure 6). The resulting titration curve first exhibits a linear increase as the dye molecules bind to the available binding sites on the ssDNA/SWNT scaffold. When there is approximately 1 dye molecule for every 4 DNA bases, the titration curve levels off indicating that the entire ssDNA/SWNT scaffold is saturated with dye molecules. The same dye to ssDNA base ratio is obtained for the dye TO-PRO-1 that is equivalent in size to YO-PRO-1 indicating that ssDNA/SWNT acts as a scaffold allowing stoichiometric self assembly of asymmetric cyanine molecules that can fit within the binding sites. On the other hand, the larger asymmetric cyanine dye TO-PRO-3 did not lead to enhanced fluorescence when titrated into ssDNA/SWNT scaffold although the wavelength of maximum emission exhibited a bathochromic shift (SI Figure 5). Presumably due to the longer methine bridge, TO-PRO-3 molecules did not appropriately fit into available binding sites on the ssDNA/SWNT scaffold. Instead, they exhibited a different binding mode than the monomethine dyes like YO-PRO-1 and TO-PRO-1 and formed aggregates on the ssDNA/SWNT scaffold as indicated by the bathochromic shift. When the same titration was performed with the dimeric form of the YO-PRO-1, namely with YOYO-1, the fluorescence intensity started to level off when there is 1 dye molecule for every 8 DNA bases which corresponds to the same dye to DNA base ratio as for the monomeric form of the dye. This result further confirms the quantitative binding of dye molecules and demonstrates that the ssDNA/SWNT acts as a predefined scaffold for the binding of asymmetrical cyanine dyes in a mode that is similar to the intercalation of the same dyes between base pairs of double stranded DNA. Asymmetrical cyanine dyes probably intercalate between the sidewalls of SWNTs and aromatic bases of ssDNA through π- π stacking interactions. When YO-PRO-1 molecules intercalate into double stranded DNA, the ratio of DNA bases to dye molecules is 2, meaning the dye molecule can bind to every other base pair[42]. As it turns out, ssDNA/SWNT scaffold has less available binding sites for asymmetrical cyanine dyes as compared to a double stranded DNA scaffold, but it is still an appropriate medium for dyes to have several fold increase in quantum yield.

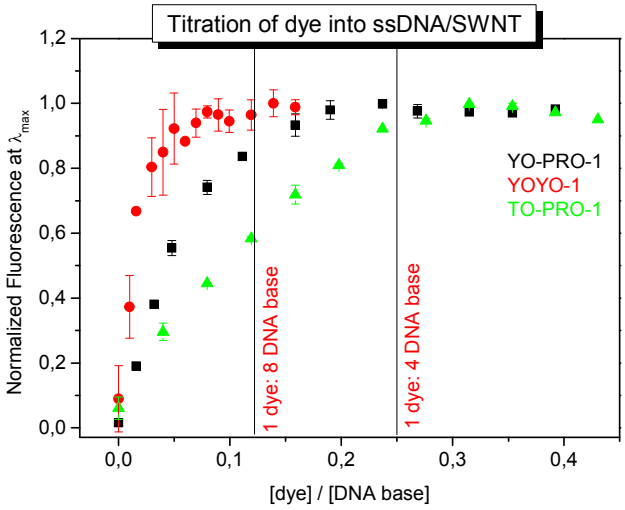

Figure 6 Titration curves obtained from titration of aliquots of dye solutions into a solution of ssDNA/SWNT scaffold containing 5μM DNA bases. Fluorescence at 512 nm, 512 nm, and 540 nm are plotted for YO-PRO-1, YOYO-1, and TO-PRO-1, respectively. The fluorescence is normalized by dividing by the maximum emission.

3.4 Thermal stability of ssDNA/SWNT/dye nanohybrids:

The thermal stability of ssDNA/SWNT/dye nanohybrids was investigated by temperature dependent fluorescence intensity measurements. Solutions of nanohybrids were heated from room temperature to 90 ^{0}C followed by a cooling cycle at a constant rate as the fluorescence at the emission maximum of the nanohybrid was monitored. The fluorescence of the hybrid was found to remain constant up to a certain temperature after which the fluorescence was decayed. It is presumed that the hybrid structure is destroyed at this temperature and the free dye that is not bound to the SWNT/DNA scaffold anymore could not exhibit fluorescence. Figure 7A shows that the ssDNA/SWNT/YO-PRO-1 hybrid structure undergoes a cooperative transition at 61^{0}C indicating the presence of one fully assembled nanostructure. The heating curve was not reproduced during cooling stage indicating that the hybrid structure was destroyed irreversible possibly due to the loss of interactions between CNT and ssDNA leading to agglomerated SWNTs. This assumption was validated by visually inspecting the appearance of the dispersion before and after the thermal cycle. While SWNTs were well dispersed before the thermal cycle, they became visible in the aggregated form after the thermal cycle (Figure 7B). It is clear that above the transition temperature dye, ssDNA, and SWNT molecules dissociate and when the temperature decreases again, only ssDNA and dye molecules can self-assemble since SWNTs are no longer available in the agglomerated form.

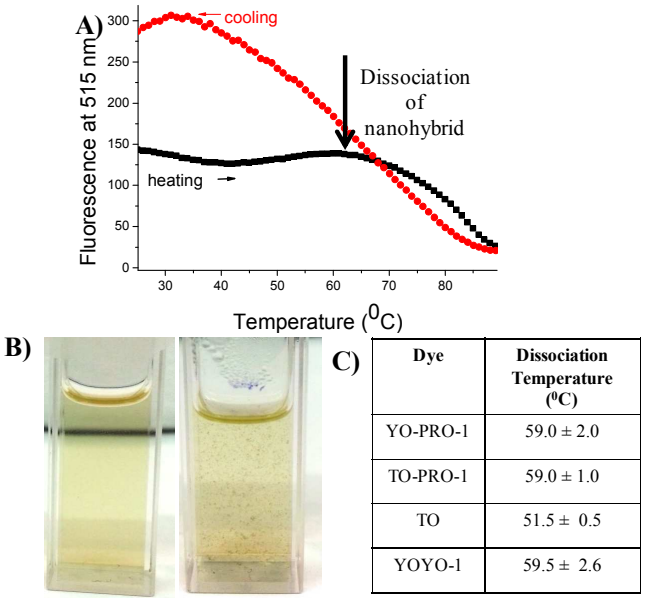

Dye	Dissociation Temperature (^{0}C)
YO-PRO-1	59.0 ± 2.0
TO-PRO-1	59.0 ± 1.0
TO	51.5 ± 0.5
YOYO-1	59.5 ± 2.6

Figure 7 A) Fluorescence intensity of ssDNA/SWNT/YO-PRO-1 nanohybrid during heating (black) and cooling (red) cycles. B) Pictures of fluorescence cuvettes at the beginning of the heating cycle (left) and at the end of the cooling cycle (right). C) Table showing the dissociation temperatures of ssDNA/SWNT/dye nanohybrids prepared by using different dyes.

To understand whether the stability of the ssDNA/SWNT/dye hybrid structure is affected by different dye molecules, thermal transitions of nanohybrids made with YOYO-1, TO-PRO-1, and TO were also investigated. Figure 7C shows the temperatures at which the ssDNA/SWNT/dye nanohybrids made with different dyes started to dissociate. While nanohybrids prepared with YO-PRO-1, TO-PRO-1 and YOYO-1 started to dissociate at approximately the same temperature, only those nanohybrids that were made with TO exhibited a lower dissociation temperature indicating a lower thermal stability. YO-PRO-1, YOYO-1 and TO-PRO-1 dyes have an extra cationic charge in their structures that is not present in TO. Presumably, these dyes interact with a higher strength with the ssDNA/SWNT scaffold due to the negatively charged ssDNA backbone, thus increasing the overall stability of the ssDNA/SWNT/dye nanohybrid structure. This result demonstrates that while the fluorescence of the nanohybrids is lost due to the dissociation of ssDNA/SWNT scaffold the structure of dye molecules arranged on the scaffold can also affect the thermal stability of these nanohybrids.

3.5 Preparation of ssDNA/SWNT/dye nanohybrids with a one step ultrasonication

Results of experiments discussed above demonstrated that mixing asymmetrical cyanine dyes with ssDNA wrapped CNTs can lead to the self-assembly of dye molecules on the CNT template, thus resulting in light emitting nanohybrid structures that are stable over increased temperatures. In order to understand whether the order of addition matters for the self-assembly of these nanohybrids we tried mixing all three components together instead of adding dye molecules into a premade ssDNA/CNT scaffold.

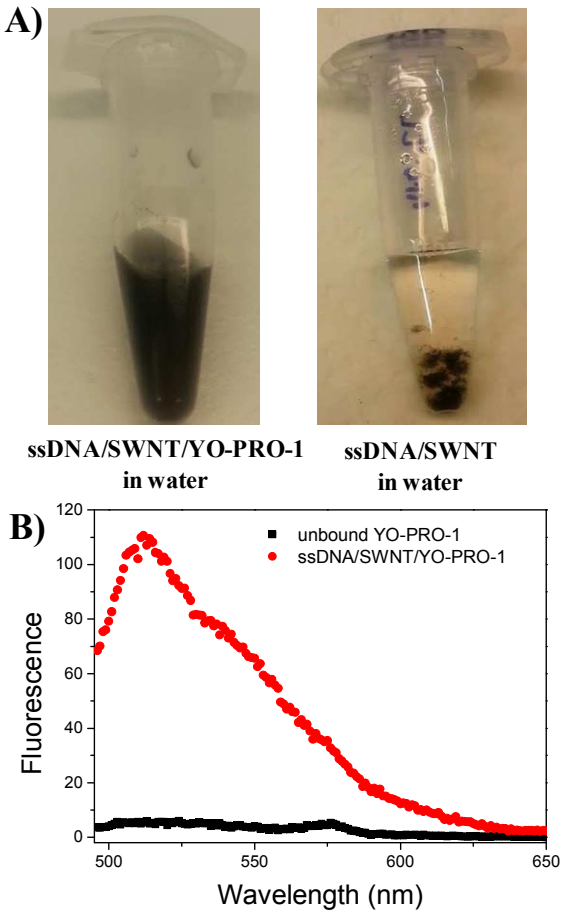

Figure 8 A) Left: Picture of the dispersion obtained after three-component sonication, aqueous solution of ssDNA, SWNT powder and aqueous YO-PRO-1 solution were probe sonicated. Right: Picture obtained after ultrasonication of ssDNA and SWNT powder. B) Fluorescence spectrum of unbound YO-PRO-1 (black) and ssDNA/SWNT/YO-PRO-1 nanohybrid obtained with three component ultrasonication.

An aqueous solution made of ssDNA, YO-PRO-1 and SWNT powder was ultrasonicated with a probe sonicator followed by ultracentrifugation to remove any SWNTs that were not dispersed. Resulting dispersion was further treated with a centrifugal filter device with a 30,000 Da cutoff membrane that allows separation of unbound dye molecules, unbound ssDNA molecules and also any ssDNA-YO-PRO-1 hybrids that are not associated with SWNTs.

Figure 8A shows the picture of the resulting dispersion. ssDNA and YO-PRO-1 molecules together allowed the debundling of SWNTs and a three-component hybrid nanostructure was self assembled again. The control experiment where the same amount of ssDNA and SWNT were sonicated in water resulted in SWNTs that were not dispersed. This result clearly demonstrates the strong dispersing effect of dye molecules on the SWNT and also proves that a three-component nanohybrid was prepared. The ssDNA/SWNT/YO-PRO-1 nanohybrids that were self-assembled through three-component sonication had similar light emitting properties as nanohybrids obtained through two-step addition. The fluorescent intensity of the nanohybrid was significantly higher than the YO-PRO-1 solution of the same concentration (Figure 8B). In this one-step mixing process there was strong competition between ssDNA/SWNT binding, ssDNA/YO-PRO-1 binding and SWNT/YO-PRO-1 binding. The fact that the fluorescent ssDNA/SWNT/YO-PRO-1 nanohybrids were obtained from this competition once more indicates that these nanohybrid structure are energetically favourable and reproducible structures rather than random assemblies.

Finally we studied weather these fluorescent nanostructures can be visualized with fluorescence microscopy. Samples of ssDNA/SWNT/YO-PRO-1 nanohybrids made via one-step mixing were prepared on a glass slide and imaged with laser scanning confocal microscope. Excitation with a 488 nm laser results in an image demonstrating strongly fluorescent structures (Figure 9A). The DSC image (Figure 9B) confirms that the fluorescence emission coincides with the location of SWNTs. While SWNTs are mainly imaged in the form of aggregates due to the way the sample was prepared, individual nanotubes could also be visualized (Figure 9C). The unique method that was developed in this study allowed turning SWNTs into fluorescent nanostructures that can be visualized with an optical microscope.

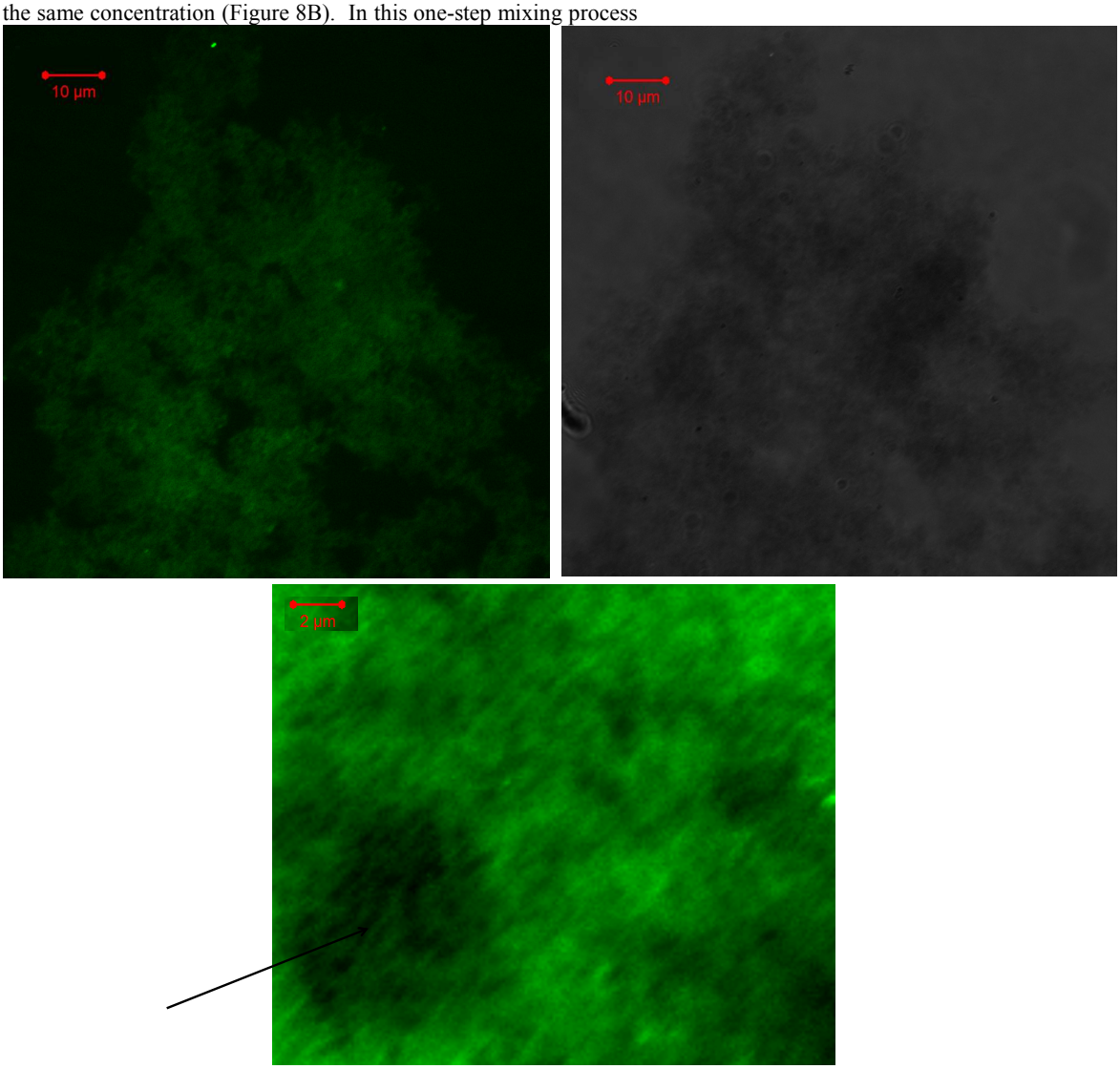

Figure 9 Confocal laser scanning microscopy images of ssDNA/SWNT/YO-PRO-1 nanohybrids A) fluorescence image, , B) The DSC image of the same spot as in A, C) Zoomed in fluorescence image.

RSC Advances

RSCPublishing

ARTICLE

4 Conclusions

We demonstrated a novel and feasible method for the preparation of light absorbing and emitting CNTs. Asymmetrical cyanine dyes were shown to interact strongly with CNTs through noncovalent binding resulting in strongly light absorbing CNT nanoarrays for which the absorption wavelength range can be tuned. When ssDNA wrapped CNTs were used as a template for the binding of same asymmetrical cyanine dyes, in addition to the enhanced light absorption, the nanoarrays were also shown to emit strong fluorescence. The ssDNA wrapped CNTs provided optimum binding sites for asymmetrical cyanine dyes to light up, thus turning CNTs into fluorescent nanostructures. For the first time, dye molecules have been demonstrated to exhibit enhanced fluorescence upon binding to CNTs which resulted in fluorescently labeled CNTs. While these asymmetrical cyanine dye/CNT hybrid structures are applicable for the detection and visualization of CNTs, they are also valuable materials as light absorbing nanoarrays with a huge potential for being utilized as light-harvesting bionanodevices and optical sensors.

Acknowledgements

This work was supported by Career Grant No: 113M144 from the Scientific and Technological Research Council of Turkey (TUBITAK).

Notes and references

[a] Sabanci University Nanotechnology Research and Application Center, Orta Mahalle Tuzla Istanbul, Turkey.

Electronic Supplementary Information (ESI) available: Absorbance spectra of MWNT/dye nanohybrids obtained with different dyes, dispersion pictures and absorbance spectra of CNT/dye hybrids obtained with different CNTs, fluorescence spectrum of MWNT/YOYO-1 nanohybrid, pictures and agarose gel images obtained during preparation of ssDNA wrapped CNTs. See DOI: 10.1039/b000000x/

References

1. D. A. Britz and A. N. Khlobystov, *Chem. Soc. Rev.*, 2006, **35**, 637-659.
2. D. Eder, *Chem Rev*, 2010, **110**, 1348-1385.
3. Y.-L. Zhao and J. F. Stoddart, *Acc. Chem. Res.*, 2009, **42**, 1161-1171.
4. S. Srinivasan and A. Ajayaghosh, in *Supramolecular Soft Matter*, John Wiley & Sons, Inc., 2011, pp. 381-406.
5. D. Jain, A. Saha and A. A. Marti, *Chem. Comm.*, 2011, **47**, 2246-2248.
6. C. Jiang, A. Saha, C. Xiang, C. C. Young, J. M. Tour, M. Pasquali and A. A. Martí, *ACS Nano*, 2013, **7**, 4503-4510.
7. D. Nepal and K. E. Geckeler, in *Advanced Nanomaterials*, Wiley-VCH Verlag GmbH & Co. KGaA, 2010, pp. 715-742.
8. E. Katz and I. Willner, *ChemPhysChem*, 2004, **5**, 1084-1104.
9. S. Marchesan and M. Prato, *Chem. Comm.,* 2015. DOI: 10.1039/c4cc09173f
10. A. Star, J. F. Stoddart, D. Steuerman, M. Diehl, A. Boukai, E. W. Wong, X. Yang, S.-W. Chung, H. Choi and J. R. Heath, *Angew. Chem. Int. Edit.*, 2001, **40**, 1721-1725.
11. S. K. Samanta, M. Fritsch, U. Scherf, W. Gomulya, S. Z. Bisri and M. A. Loi, *Acc. Chem. Res.*, 2014, **47**, 2446-2456.
12. P. Bilalis, D. Katsigiannopoulos, A. Avgeropoulos and G. Sakellariou, *RSC Advances*, 2014, **4**, 2911-2934.
13. E. Pavoni, E. Bandini, M. Benaglia, J. K. Molloy, G. Bergamini, P. Ceroni and N. Armaroli, *Polymer Chem.*, 2014, **5**, 6148-6150.
14. E. Kymakis and G. A. J. Amaratunga, *Appl. Phys. Lett.*, 2002, **80**, 112-114.
15. B. Ballesteros, G. de la Torre, C. Ehli, G. M. Aminur Rahman, F. Agulló-Rueda, D. M. Guldi and T. Torres, *J. Am. Chem. Soc.*, 2007, **129**, 5061-5068.
16. E. S. Cho, S. W. Hong and W. H. Jo, *Macromol. Rapid Commun.*, 2008, **29**, 1798-1803.
17. L. Zhang, H. Wei, J. Li, T. Li, D. Li, Y. Li and E. Wang, *Biosens. Bioelectron.*, 2010, **25**, 1897-1901.
18. N. Nakayama-Ratchford, S. Bangsaruntip, X. Sun, K. Welsher and H. Dai, *J. Am. Chem. Soc.*, 2007, **129**, 2448-2449.
19. S. H. Yoshimura, S. Khan, H. Maruyama, Y. Nakayama and K. Takeyasu, *Biomacromolecules*, 2011, **12**, 1200-1204.
20. R. Prakash, S. Washburn, R. Superfine, R. E. Cheney and M. R. Falvo, *Appl. Phys. Lett.*, 2003, **83**, 1219-1221.
21. J. Zhang, J. K. Lee, Y. Wu and R. W. Murray, *Nano Lett.*, 2003, **3**, 403-407.
22. R. B. Martin, L. Qu, Y. Lin, B. A. Harruff, C. E. Bunker, J. R. Gord, L. F. Allard and Y.-P. Sun, *J. Phys. Chem. B*, 2004, **108**, 11447-11453.
23. G. M. A. Rahman, D. M. Guldi, S. Campidelli and M. Prato, *J. Mater. Chem.*, 2006, **16**, 62-65.
24. J. P. Casey, S. M. Bachilo and R. B. Weisman, *J. Mater. Chem.*, 2008, **18**, 1510-1516.
25. B. Pan, D. Cui, C. S. Ozkan, M. Ozkan, P. Xu, T. Huang, F. Liu, H. Chen, Q. Li, R. He and F. Gao, *J. Phys. Chem. C*, 2008, **112**, 939-944.
26. V. V. Didenko, V. C. Moore, D. S. Baskin and R. E. Smalley, *Nano Lett.*, 2005, **5**, 1563-1567.
27. K. Otobe, H. Nakao, H. Hayashi, F. Nihey, M. Yudasaka and S. Iijima, *Nano Lett.*, 2002, **2**, 1157-1160.
28. W. Z. Yuan, J. Z. Sun, Y. Dong, M. Häussler, F. Yang, H. P. Xu, A. Qin, J. W. Y. Lam, Q. Zheng and B. Z. Tang, *Macromolecules*, 2006, **39**, 8011-8020.
29. B. Koh, G. Kim, H. K. Yoon, J. B. Park, R. Kopelman and W. Cheng, *Langmuir*, 2012, **28**, 11676-11686.
30. Z. Zhu, R. Yang, M. You, X. Zhang, Y. Wu and W. Tan, *Anal. Bioanal. Chem.*, 2010, **396**, 73-83.
31. C. F. Chiu, N. Dementev and E. Borguet, *J. Phys. Chem. A*, 2011, **115**, 9579-9584.

32. H. S. Rye, S. Yue, D. E. Wemmer, M. A. Quesada, R. P. Haugland, R. A. Mathies and A. N. Glazer, *Nucleic Acids Res.*, 1992, **20**, 2803-2812.
33. G. L. Silva, V. Ediz, D. Yaron and B. A. Armitage, *J. Am. Chem. Soc.*, 2007, **129**, 5710-5718.
34. A. S. Tatikolov, *J. Photochem. Photobiol. C: Photochem. Rev.*, 2012, **13**, 55-90.
35. H. Özhalıcı-Ünal and B. A. Armitage, *ACS Nano*, 2009, **3**, 425-433.
36. H. Özhalici-Ünal, C. L. Pow, S. A. Marks, L. D. Jesper, G. L. Silva, N. I. Shank, E. W. Jones, J. M. Burnette, P. B. Berget and B. A. Armitage, *J. Am. Chem. Soc.*, 2008, **130**, 12620-12621.
37. A. Fürstenberg and E. Vauthey, *J. Phys. Chem. B*, 2007, **111**, 12610-12620.
38. A. Mandal and A. K. Nandi, *J. Phys. Chem. C*, 2012, **116**, 9360-9371.
39. D. Baskaran, J. W. Mays and M. S. Bratcher, *Chem. Mater.*, 2005, **17**, 3389-3397.
40. M. Zheng, A. Jagota, E. D. Semke, B. A. Diner, R. S. McLean, S. R. Lustig, R. E. Richardson and N. G. Tassi, *Nat. Mater.*, 2003, **2**, 338-342.
41. Y. Li, X. Han and Z. Deng, *Angew. Chem.*, 2007, **119**, 7625-7628.
42. L. G. Lee, C.-H. Chen and L. A. Chiu, *Cytometry*, 1986, **7**, 508-517.

